Nonadiabatic Interactions in the Cl + H2 Reaction Probed by ClH 2- and ClD2- Photoelectron Imaging

Etienne Garand, *et al.*

Science **319**, 72 (2008);
DOI: 10.1126/science.1150602

Nonadiabatic Interactions in the Cl + H_2 Reaction Probed by ClH_2^- and ClD_2^- Photoelectron Imaging

Etienne Garand,[1] Jia Zhou,[1] David E. Manolopoulos,[2]* Millard H. Alexander,[3]* Daniel M. Neumark[1,4]*

The degree of electronic and nuclear coupling in the Cl + H_2 reaction has become a vexing problem in chemical dynamics. We report slow electron velocity-map imaging (SEVI) spectra of ClH_2^- and ClD_2^-. These spectra probe the reactant valley of the neutral reaction potential energy surface, where nonadiabatic transitions responsible for reactivity of the Cl excited spin-orbit state with H_2 would occur. The SEVI spectra reveal progressions in low-frequency Cl·H_2 bending and stretching modes, and are compared to simulations with and without nonadiabatic couplings between the Cl spin-orbit states. Although nonadiabatic effects are small, their inclusion improves agreement with experiment. This comparison validates the theoretical treatment, especially of the nonadiabatic effects, in this critical region of the Cl + H_2 reaction, and suggests strongly that these effects are minor.

The Cl + H_2 → HCl + H reaction has been studied for more than a century, serving as a benchmark for the development of bimolecular reaction rate theory (*1*). It has attracted renewed attention over the past decade, as fresh theoretical and experimental results have highlighted unanticipated features of the reaction and challenged our fundamental understanding of its dynamics. In particular, a study of the Cl + HD reaction by Skouteris *et al*. (*2*) provided experimental evidence that the weak van der Waals (vdW) forces in the reactant valley have a notable effect on the branching ratio of the HCl:DCl product as a function of collision energy. These results suggest that spectroscopic study of the prereactive Cl·H_2 complex would provide new insights into how weak vdW interactions affect chemical reactivity.

Such an experiment would also shed light on an important ongoing controversy concerning the relative reactivities of ground-state Cl($^2P_{3/2}$) and excited spin-orbit state Cl*($^2P_{1/2}$), lying 882.3 cm^{-1} higher, measured in crossed molecular beam experiments by Liu and co-workers (*3*, *4*). For reactions of Cl or F with H_2, only the X($^2P_{3/2}$) state correlates adiabatically with the HX + H products in their electronic ground state. Experience shows that the Born-Oppenheimer (BO) approximation will govern chemical reactions, so that the electronically adiabatic pathway should always dominate (*5*, *6*). This is confirmed by multi–potential energy surface (PES) reactive scattering calculations on the F + H_2 (*7*) and Cl + H_2 (*8*, *9*) systems by Alexander *et al*., and, most convincingly, in a recent comparison with crossed molecular beam experiments by Yang and co-workers (*10*) on the F + D_2 system. In that comparison, the calculations were based on a highly correlated, scaled set of PESs in which the experimental exoergicity and the presumed experimental barrier height were accurately reproduced. Only at very low collision energies, where the reaction barrier quenches the BO-allowed F + D_2 reaction, did the BO-forbidden F* + D_2 reaction become comparable in relative importance. In contrast, the experiments of Liu and co-workers imply that the exact opposite is true for the Cl/Cl* + H_2 reaction: At low energy, the BO-allowed reaction dominates, but as the collision energy increases, the BO-forbidden reaction becomes increasingly important. These results can be explained only by postulating that nonadiabaticity in the Cl + H_2 reaction is qualitatively different from that in the F + H_2 reaction and in the quantum simulations of the Cl + H_2 reaction. This difference—and, in particular, the discrepancy between experiment and theory—is currently one of the major unresolved problems in chemical reaction dynamics.

With these considerations in mind, we report high-resolution photoelectron imaging spectra of ClH_2^- and ClD_2^-. This experiment spectroscopically probes the prereactive complex of the Cl + H_2 reaction, offering complementary information to Liu's reactive scattering experiments, in precisely the region where the nonadiabatic transitions responsible for the reactivity of the Cl*($^2P_{1/2}$) state are expected to occur (*7*–*9*, *11*, *12*). The experimental results are compared with two separate sets of Franck-Condon (FC) simulations in which the nonadiabatic coupling between the Capecchi-Werner ab initio PESs (*13*) is first neglected and then retained.

Photoelectron spectroscopy of anionic complexes has been used to probe the transition states of bimolecular reactions (*14*, *15*). A notable example of this transition-state spectroscopy was a study of the FH_2^- anion, whose ground-state geometry has good FC overlap with the early barrier of the F + H_2 reaction (*16*, *17*). In contrast, the Cl + H_2 reaction has a later barrier, and thus the equilibrium geometry of ClH_2^- is much closer to the reactant valley than to the transition state (Fig. 1). The ClH_2^- anion wave function has good FC overlap with the vibrational and hindered rotor states of the neutral Cl·H_2 vdW complex (*18*); with an energy resolution of 1 meV, it was predicted that several features associated with bound and resonance states of this prereactive complex could be resolved (*18*).

Photoelectron spectra of ClH_2^- and ClD_2^- obtained with a conventional negative ion time-of-flight photoelectron spectrometer have been reported (*19*). These spectra exhibited features associated with the spin-orbit splitting in the Cl·H_2 complex. However, finer structures associated with vibrations and hindered rotor motions of the complex could not be observed because of the limited resolution, around 8 to 10 meV. Recently, Osterwalder *et al*. (*20*) developed slow electron velocity-map imaging (SEVI), which combines the high collection efficiency of velocity-map

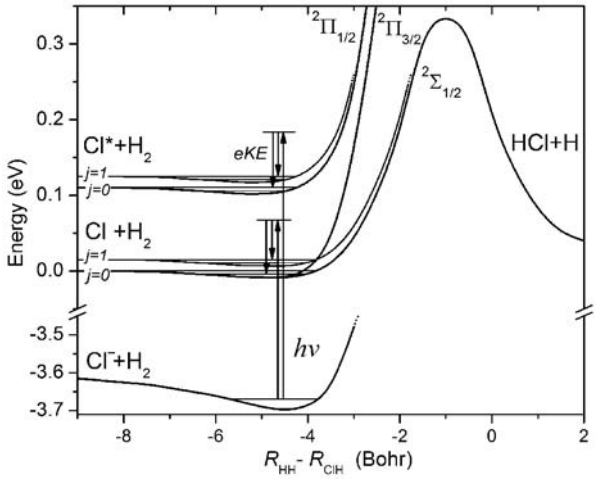

Fig. 1. Schematic view of the Cl·H_2 anionic and neutral PESs in terms of relative distance between the atoms. Photodetachment of ClH_2^- probes the shallow vdW wells in the entrance valley of the Cl + H_2 reaction, where the nonadiabatic transitions responsible for the reactivity of the Cl*($^2P_{1/2}$) state are expected to occur.

[1]Department of Chemistry, University of California, Berkeley, CA 94720, USA. [2]Physical and Theoretical Chemistry Laboratory, Oxford University, South Parks Road, Oxford OX1 3QZ, UK. [3]Department of Chemistry and Biochemistry and Institute for Physical Science and Technology, University of Maryland, College Park, MD 20742, USA. [4]Chemical Sciences Division, Lawrence Berkeley National Laboratory, Berkeley, CA 94720, USA.

*To whom correspondence should be addressed. E-mail: david.manolopoulos@chem.ox.ac.uk (D.E.M.); mha@umd.edu (M.H.A.); dneumark@berkeley.edu (D.M.N.)

imaging (VMI) (*21*, *22*) with the high resolution of threshold photodetachment. In this technique, mass-selected anions generated from a pulsed molecular beam are photodetached at energies slightly above threshold by means of a tunable dye laser. The resulting slow photoelectrons are extracted collinearly with the ion beam by a VMI assembly and mapped onto imaging microchannel plates coupled to a phosphor screen. High-resolution photoelectron spectra are obtained by angular integration of the inverse-Abel transformed images. All the observed transitions have similar widths in electron velocity, so the resolution scales as the square root of the electron kinetic energy. The highest resolution, up to 1 cm^{-1} for atomic anions, is obtained at wavelengths close to the threshold for a particular photodetachment transition, whereas lower-resolution spectra with wider energy windows can be measured by operating further from threshold (*23*).

Preliminary SEVI spectra (*20*) of ClD_2^- resolved more structure than was seen in the photoelectron spectra. However, by shortening the electron flight tube to minimize the effect of stray fields and using an Even-Lavie pulsed valve with a pulsed ionizer (*24*) and higher backing pressure [250 psi total, using trace CCl_4 in a 10:1 Ar:H_2(D_2) mix] to produce colder anions, we have improved on the resolution of this earlier study, finding many previously unseen features that allow for rigorous comparison with theory.

Overview SEVI spectra of ClH_2^- and ClD_2^- taken at wavelengths of 326.5 nm and 323.0 nm, respectively, are shown in Fig. 2. The $^{37}ClH_2^-$ isotopolog was chosen to avoid interference from photodetachment of $^{37}Cl^-$, which produces photoelectrons in the same energy range; for ClD_2^-, the more abundant $^{35}ClD_2^-$ was used. The SEVI spectrum of Cl^- taken at 325 nm, acquired for calibration, is shown in the bottom panel of Fig. 2 for comparison. The ClH_2^- and ClD_2^- spectra are dominated by two main features associated with the spin-orbit states of the chlorine atom. Although these features already show more structure than was seen previously, the resolution of the SEVI spectra can be improved further by tuning the detachment laser just above the threshold of the feature of interest.

This procedure yields the spectra of the two spin-orbit features of ClH_2^- and ClD_2^- in Figs. 3 and 4, respectively. These higher-resolution spectra reveal several new features. For example, in Fig. 2, the shoulder and first two peaks in the $Cl(^2P_{3/2})$·D_2 band appear as five features in the top panel of Fig. 4, with the two peaks each being split into closely spaced doublets.

As shown in Fig. 1, the interaction of Cl and Cl* with H_2 ($^1\Sigma_g^+$) gives rise to three adiabatic electronic PESs, labeled $^2\Sigma_{1/2}$, $^2\Pi_{3/2}$, and $^2\Pi_{1/2}$, in linear geometries (*25*). In the adiabatic limit, only $Cl(^2P_{3/2})$ atoms that approach H_2 on the $^2\Sigma_{1/2}$ PES react to form ground-state products. Figure 1 also shows that each electronic state has bend/hindered rotor levels that correlate to various H_2 rotational levels j (only j = 0 and 1 are shown) and that each bend level has a shallow vdW well that supports very-low-frequency Cl·H_2 stretching vibrations.

The spectra in Figs. 3 and 4 can be fully assigned, on the basis of electronically adiabatic FC simulations of detachment, to the three neutral states. The dashed lines in Figs. 3 and 4 show the simulated spectra obtained using the coupled-cluster [CCSD(T)] PES of Alexander (*26*) for the anion and retaining all three electronically adiabatic PESs of Capecchi and Werner (*13*) for the neutral, as described in (*18*). None of the nonadiabatic couplings were included. The simulated spectra assume the usual ortho:para ratio of 3:1 for ClH_2 and 2:1 for ClD_2. (The rotational quantum number j is even for p-H_2 and o-D_2 and odd for o-H_2 and p-D_2.) Because the intensity of the experimental signal is arbitrary, the experimental and calculated intensities have been scaled to give the same maximum peak height in each panel. The theoretical spectra were also shifted slightly to match the position of the origin transition in Cl·H_2 (29,533 cm^{-1}) and Cl·D_2 (29,631 cm^{-1}). This shift was the only adjustable parameter used in the simulations.

In the top panel of Fig. 3, the observed peaks are associated with the hindered H_2(j = 0 and 1) rotor states of the weakly bound Cl·H_2 complex on the ground $^2\Sigma_{1/2}$ electronic PES. One quantum of excitation in the Cl·H_2 vdW stretching vibration (ν_s) is also observed at 30 cm^{-1} above the (j = 1, ν_s = 0) level. These quantum numbers can be unambiguously assigned by means of a simple adiabatic-bender analysis (*27*, *28*). Transitions to the vdW bound and resonance states associated with the $^2\Pi_{3/2}$ electronic state are predicted to have lower intensities, owing to poorer FC overlap with the anion wave function, and are buried beneath these $^2\Sigma_{1/2}$ transitions (*18*). The peak marked with an asterisk at 29,495 cm^{-1} lies 153 cm^{-1} below the (j = 1, ν_s = 0) peak. Because this shift is close to the measured stretching vibration in the anion (*26*), we assign this peak to a hot band originating from the anion ν_s = 1 state. Finally, the two features in the bottom panel of Fig. 3 are assigned to the (j = 1, ν_s = 0) and (j = 1, ν_s = 1) vdW bend-stretch states on the $^2\Pi_{1/2}$ excited electronic state.

The ClD_2^- spectrum exhibits similar features but with a smaller hindered rotor spacing. In the top panel of Fig. 4, the observed transitions are assigned to hindered D_2 rotor modes (j = 0, 1, 2) on the $^2\Sigma_{1/2}$ ground electronic state, with a 30 cm^{-1} stretching vibration resolved for the j = 1 and 2 levels. Similar transitions are observed on the $^2\Pi_{1/2}$ electronic state and are shown in the bottom panel of Fig. 4.

Although the electronically adiabatic simulations in Figs. 3 and 4 allow us to assign most features in the measured spectra, there are some clear differences (on the order of 10 cm^{-1}) between several of the predicted peak positions and those observed experimentally. To address these discrepancies, we performed a second set of FC simulations in which the dynamics of the neutral

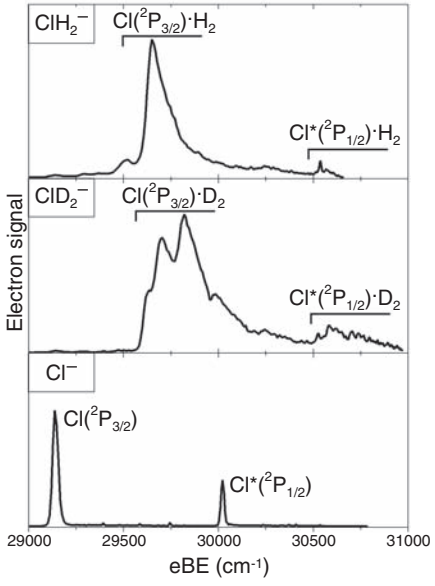

Fig. 2. Overview SEVI spectra of ClH_2^- (**top**) and ClD_2^- (**middle**) taken at wavelengths of 326.5 nm and 323 nm, respectively. The SEVI spectrum of Cl^- (**bottom**) taken at 325 nm is shown for comparison. All spectra show electron signal as a function of electron binding energy (eBE), defined as the difference between the photon energy and the measured electron kinetic energy.

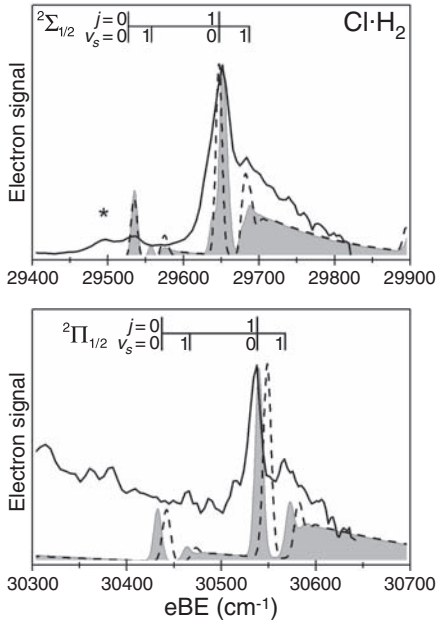

Fig. 3. High-resolution SEVI spectrum of ClH_2^- (solid line) is compared with FC simulations where the nonadiabatic interactions are neglected (dashed line) and included (gray-shaded area). Both spectra show electron signal as a function of eBE, defined as in Fig. 2. (**Top**) Average of three spectra taken between 334.5 and 335.5 nm; (**bottom**) average of three spectra taken between 326 and 326.5 nm.

ClH_2 complex were described by the same Hamiltonian used by Alexander *et al.* in their multi-PES quantum reactive scattering calculations for $Cl + H_2$ (*8*, *9*). This treatment includes four quasi-diabatic PESs as well as the spin-orbit and Coriolis coupling between the electronic-rovibrational states (*7*).

In modeling the photodetachment process, we assumed as in our adiabatic simulations that the ClH_2^- anion was sufficiently rotationally cold to be modeled by total angular momentum $J = 0$. We also exploited the Wigner threshold law for anion photodetachment (*29*, *30*), which implies that the dominant excitation pathway at sufficiently low electron kinetic energies will be the excitation of a Cl 3p electron to a continuum s orbital. Allowing for the angular momenta of the incident photon and the departing photoelectron, these assumptions lead to independent excitation of the $J = 1/2$ and $J = 3/2$ angular momentum states of $Cl{\cdot}H_2$, corresponding to the excitation of $Cl(^2P_{1/2}){\cdot}H_2$ and $Cl(^2P_{3/2}){\cdot}H_2$, respectively.

The neutral angular momentum states $\Psi^{JM}_{\text{neutral}}$ were constructed by dressing the anion vibrational wave function ψ^{00}_{anion} with appropriate linear combinations of Wigner rotation matrix elements $D^{J*}_{MK}(\Omega)$ (to describe the rotational motion of the triatomic complex) and $Cl(^2P)$ atom electronic states $|JK\rangle$, with equal amplitudes for each of the $(2J + 1)$ projections of J on the Cl-H_2 axis, as represented by

$$\Psi^{JM}_{\text{neutral}} = \left(\frac{2J+1}{4\pi}\right)^{1/2} \sum_{K=-J}^{J} D^{J*}_{MK}(\Omega)|JK\rangle\psi^{00}_{\text{anion}} \quad (1)$$

where K and M are the projections of J on the body- and space-frame z axes, and Ω denotes the set of Euler angles used to transform between the two frames.

The FC spectrum, given by

$$P^J(E) = \langle\Psi^{JM}_{\text{neutral}}|\delta(E - H)|\Psi^{JM}_{\text{neutral}}\rangle \quad (2)$$

was then calculated using the time-dependent wave packet method with absorbing boundary conditions described in (*18*), but now including electrostatic, spin-orbit, and Coriolis coupling between the diabatic electronic states (*7*). The gray-shaded spectra superimposed in Figs. 3 and 4 are the predicted photoelectron spectra for normal ClH_2^- and ClD_2^- when these nonadiabatic couplings are retained.

Alexander *et al.* (*9*) have shown that the main nonadiabatic effect in the $Cl + H_2$ reaction is the coupling between the $^2\Sigma_{1/2}$ and $^2\Pi_{1/2}$ electronic states induced by the spin-orbit Hamiltonian. The effect of this coupling will be strongest when the splitting between the $^2\Sigma$ and $^2\Pi$ states, independent of spin-orbit coupling, is comparable to the magnitude of the spin-orbit coupling. The point at which these two are equivalent in magnitude occurs close to the bottom of the prereactive vdW well probed in this study (*9*). In addition, because all of the transitions resolved here correspond to photodetachment to the $^2\Sigma_{1/2}$ and $^2\Pi_{1/2}$ states (recall that transitions to the bend-stretch levels associated with the $^2\Pi_{3/2}$ state have poorer FC overlap with the anion), the effect of this spin-orbit coupling, if large, should be directly observable. However, it can be seen from Figs. 3 and 4 that the inclusion of nonadiabatic effects in the FC simulation induces only subtle changes in the calculated spectra.

The most noticeable difference between the two simulations is the reduction, when the nonadiabatic coupling is retained, of the splitting between the bend-stretch levels associated with the $^2\Sigma_{1/2}$ and $^2\Pi_{1/2}$ states. For example, in the ClH_2 spectra, the splitting between the ($j = 1$, $v_s = 0$) levels associated with these two states is reduced from 902 to 888 cm^{-1}, in excellent agreement with the value of 887 cm^{-1} found experimentally. Similarly, in ClD_2, the spacing between the ($j = 0$, $v_s = 0$) levels is reduced from 908 to 900 cm^{-1}, which exactly matches the experimental spectrum. These reductions can be explained in terms of small changes in the shapes of the adiabatic-bender potentials induced by the spin-orbit, Coriolis, and electrostatic couplings, which result in changes in the energies of the bend-stretch vdW levels in the two electronic states.

The bottom panels of Figs. 3 and 4 also show that the widths of the peaks from the two sets of simulations are comparable. The $^2\Pi_{1/2}$ states can decay by nonadiabatic coupling to the lower $^2\Sigma_{1/2}$ states, but only if nonadiabatic coupling is included. If the magnitude of nonadiabatic couplings were large, the peaks would be significantly broadened in the fully coupled calculation. This is not observed.

The effect of including the nonadiabatic coupling can be seen more clearly in the ClD_2^- spectra, which display a denser vibrational structure owing to the larger mass of the deuterium atom. In the lower $^2\Sigma_{1/2}$ state, relative to the adiabatic simulation, the hindered rotor spacing is slightly increased and the $v_s = 1$ level lies closer to the dissociative continuum. Overall, the effects of nonadiabatic coupling are small, but their incorporation into the simulations results in a noticeably better match with the high-resolution SEVI spectra.

The comparison between experimental and calculated spectra shown in Figs. 3 and 4 leads to two important conclusions regarding the $Cl + H_2$ reaction. First, the level of agreement of both sets of simulations with the experimental spectra validates the accuracy of the Capecchi-Werner PESs in the region of the vdW well in the reactant valley. This validation is important because the weak interactions that give rise to this well play a decisive role in determining the product branching ratio of the Cl + HD reaction (*2*). Second, our results show that the effects of non-BO couplings in the prereactive region have been correctly evaluated in the theoretical simulation, to nearly spectroscopic (1 cm^{-1}) accuracy.

The present treatment of the nonadiabatic electronic-vibrational-rotational motion of the ClH_2 system is based on the same Hamiltonian as was used in the quantum reactive scattering calculations of Alexander *et al.* (*8*). Hence, the good agreement found here tends to support the prediction of these calculations that the adiabatic $Cl + H_2$ reaction pathway will dominate as the collision energy increases. In principle, we expect that the sophisticated ab initio techniques used by Capecchi and Werner (*13*) for the determination of the ClH_2 PESs should be as accurate as those used for the FH_2 system, for which theory and experiment agree on the extent of nonadiabaticity (*10*). Ultimately, the disagreement between these reactive scattering calculations (*8*) and earlier experimental work (*3*, *4*) may demand a new experimental investigation of this reaction.

Finally, our results show that the SEVI technique can yield vibrationally resolved spectra of weakly bound vdW complexes. This method has considerable promise for studies of bimolecular reactions involving polyatomic reactants such as $F + CH_4$ and $Cl + CH_4$. The reactive resonances reported recently for these reactions (*31*, *32*) should be spectroscopically accessible if SEVI is used.

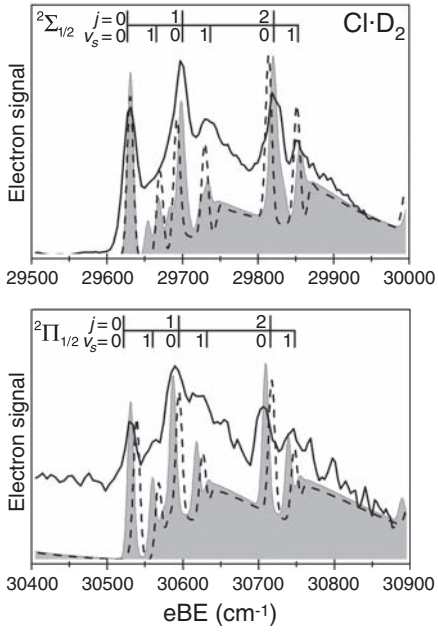

Fig. 4. High-resolution SEVI spectrum of ClD_2^- (solid line) is compared with FC simulations where the nonadiabatic interactions are neglected (dashed line) and included (gray-shaded area). Both spectra show electron signal as a function of eBE. (**Top**) Average of three spectra taken between 333 and 334 nm; (**bottom**) average of three spectra taken between 323 and 324 nm.

References

1. M. Alagia *et al.*, *Science* **273**, 1519 (1996).
2. D. Skouteris *et al.*, *Science* **286**, 1713 (1999).
3. F. Dong, S. H. Lee, K. Liu, *J. Chem. Phys.* **115**, 1197 (2001).

4. S. H. Lee, K. P. Liu, *J. Chem. Phys.* **111**, 6253 (1999).
5. P. J. Dagdigian, M. L. Campbell, *Chem. Rev.* **87**, 1 (1987).
6. R. J. Donovan, *Chem. Rev.* **70**, 489 (1970).
7. M. H. Alexander, D. E. Manolopoulos, H.-J. Werner, *J. Chem. Phys.* **113**, 11084 (2000).
8. M. H. Alexander, G. Capecchi, H.-J. Werner, *Science* **296**, 715 (2002).
9. M. H. Alexander, G. Capecchi, H.-J. Werner, *Faraday Disc.* **127**, 59 (2004).
10. L. Che *et al.*, *Science* **317**, 1061 (2007).
11. E. E. Nikitin, *Theory of Elementary Atomic and Molecular Processes in Gases* (Clarendon, Oxford, 1974).
12. V. Aquilanti, G. Grossi, *J. Chem. Phys.* **73**, 1165 (1980).
13. G. Capecchi, H.-J. Werner, *Phys. Chem. Chem. Phys.* **6**, 4975 (2004).
14. D. M. Neumark, *Phys. Chem. Chem. Phys.* **7**, 433 (2005).
15. D. M. Neumark, *J. Chem. Phys.* **125**, 132303 (2006).
16. S. E. Bradforth, D. W. Arnold, D. M. Neumark, D. E. Manolopoulos, *J. Chem. Phys.* **99**, 6345 (1993).
17. D. E. Manolopoulos *et al.*, *Science* **262**, 1852 (1993).
18. D. E. Manolopoulos, M. H. Alexander, *Phys. Chem. Chem. Phys.* **6**, 4984 (2004).
19. M. J. Ferguson, G. Meloni, H. Gomez, D. M. Neumark, *J. Chem. Phys.* **117**, 8181 (2002).
20. A. Osterwalder, M. J. Nee, J. Zhou, D. M. Neumark, *J. Chem. Phys.* **121**, 6317 (2004).
21. D. W. Chandler, P. L. Houston, *J. Chem. Phys.* **87**, 1445 (1987).
22. A. Eppink, D. H. Parker, *Rev. Sci. Instrum.* **68**, 3477 (1997).
23. J. Zhou, E. Garand, W. Eisfeld, D. M. Neumark, *J. Chem. Phys.* **127**, 034304 (2007).
24. U. Even, J. Jortner, D. Noy, N. Lavie, C. Cossart-Magos, *J. Chem. Phys.* **112**, 8068 (2000).
25. V. Aquilanti, S. Cavalli, F. Pirani, A. Volpi, D. Cappelletti, *J. Phys. Chem. A* **105**, 2401 (2001).
26. M. H. Alexander, *J. Chem. Phys.* **118**, 9637 (2003).
27. S. L. Holmgren, M. Waldman, W. Klemperer, *J. Chem. Phys.* **67**, 4414 (1977).
28. M. H. Alexander, S. Gregurick, P. J. Dagdigian, *J. Chem. Phys.* **101**, 2887 (1994).
29. R. C. Bilodeau, M. Scheer, H. K. Haugen, *Phys. Rev. Lett.* **87**, 143001 (2001).
30. E. P. Wigner, *Phys. Rev.* **73**, 1002 (1948).
31. W. Shiu, J. J. Lin, K. P. Liu, *Phys. Rev. Lett.* **92**, 103201 (2004).
32. B. Zhang, K. Liu, *J. Chem. Phys.* **122**, 101102 (2005).

17 September 2007; accepted 1 November 2007
10.1126/science.1150602

Helium and Neon Abundances and Compositions in Cometary Matter

Bernard Marty,[1] Russell L. Palma,[2,3] Robert O. Pepin,[3]* Laurent Zimmermann,[1] Dennis J. Schlutter,[3] Peter G. Burnard,[1] Andrew J. Westphal,[4] Christopher J. Snead,[4] Saša Bajt,[5] Richard H. Becker,[3] Jacob E. Simones[2]

Materials trapped and preserved in comets date from the earliest history of the solar system. Particles captured by the Stardust spacecraft from comet 81P/Wild 2 are indisputable cometary matter available for laboratory study. Here we report measurements of noble gases in Stardust material. Neon isotope ratios are within the range observed in "phase Q," a ubiquitous, primitive organic carrier of noble gases in meteorites. Helium displays ^{3}He/^{4}He ratios twice those in phase Q and in Jupiter's atmosphere. Abundances per gram are surprisingly large, suggesting implantation by ion irradiation. The gases are probably carried in high-temperature igneous grains similar to particles found in other Stardust studies. Collectively, the evidence points to gas acquisition in a hot, high ion-flux nebular environment close to the young Sun.

Comets are frozen, largely unaltered reservoirs of dust and gases present in the early solar nebula. They are likely to contain well-preserved records of the chemical, mineralogic, and isotopic character of primordial solar-system matter. On 15 January 2006, the Stardust Mission returned to Earth with a cargo of particles collected from the coma of comet 81P/Wild 2 (*1*). These not only open the door to detailed laboratory investigation of the nature of cometary matter, but will also provide chemical, mineralogic, and isotopic markers for identifying samples of comets suspected to be already present in extraterrestrial material collections [e.g., (*2*–*6*)].

Noble gases are excellent tracers of contributions from various solar-system volatile reservoirs and of physical processing of gases acquired from these reservoirs. Their elemental and isotopic compositions in primitive meteorites differ from those in the Sun, as represented by the solar wind. Planetary atmospheres display noble gas signatures distinct from both solar and meteoritic patterns. A detailed knowledge of cometary noble gas abundances and isotopic compositions, unknown before Stardust, will allow investigation of compositional links between comets, the solar nebula, primitive meteorites for which a cometary origin has been advocated (*7*, *8*), micrometeorites and interplanetary dust particles (IDPs), and the atmospheres of Earth, Mars, and Venus, where contributions of noble gases carried by comets have been proposed and debated (*9*–*11*).

The Wild 2 particles were collected by Stardust in aerogel, a porous low-density silica glass designed to decelerate an impacting grain with minimal alteration (*1*). The material analyzed in this study was extracted from the bulbous cavity wall of the capture track shown in Fig. 1A. We report results of helium and neon measurements on five subsamples of this material [Fig. 1B and fig. S1 (*12*)], carried out independently, using different extraction and analytical methods, at Centre de Recherches Pétrographiques et Géochimiques (CRPG) Nancy, France, and the University of Minnesota, Minneapolis, USA (*13*). Gases were thermally released from the five samples, two (Thera-1 and Thera-2) at CRPG by single-step laser melting and three (St-1, St-2, St-3) at Minnesota by multistep pyrolysis to ~1400°C. Evolved He and Ne abundances were not large, in some cases exceeding blank levels by factors of only 2 to 3, and so accurate assessments of aerogel and instrumental blanks were crucial. Details on blank determinations, and other discussions of materials and methods, are set out in (*12*).

The bulbous track-wall samples are mixtures of aerogel and small grains shed from the impacting particle. Gases were held very retentively in their host grains; temperatures above ~1250°C (±50°C) were required to degas He and Ne in the Minnesota step-heating procedure. Originally we thought that gases might have been liberated by flash heating of the incident particle in the upper part of its deceleration track (Fig. 1A) and trapped in melted aerogel that rapidly chilled to silica glass along the track walls. It is now clear that the ~1200° to 1250°C temperatures reached before initiation of release (*12*) are incompatible with siting in aerogel. Diffusion coefficients for He in vitreous silica (*14*) are so large at these temperatures that glassy aerogel would empty itself in ~10 s—comparable to step heating times—even if diffusion distances were comparable to the 1-mm sample dimensions (Fig. 1B and fig. S1), and much more quickly (<1 s) at the ≤100-μm scale. Observed release profiles instead point to gas siting in refractory grains. This inference is consistent with the bulb-wall mineralogy measured by x-ray absorption spectroscopy (supporting online text), indicating that the grains are composed primarily (~75% by mass) of high-temperature metal (FeNi), metal-sulfur, and metal-carbon minerals. The remaining 25% are mostly silicates together with unidentified components. A separate search for carbon compounds was carried out by infrared (IR) spectroscopy (supporting online text) to address the possibility that the gas carriers might be refractory organic materials. None were detected. However, the search covered only a small fraction of the bulb wall and adjacent aerogel, so the presence of heterogeneously distributed organics is not ruled out. We return to the issue of the nature of the gas carrier later in the paper.

[1]Centre de Recherches Pétrographiques et Géochimiques, Nancy Université, BP 20, 54501 Vandoeuvre-lès-Nancy Cedex, France. [2]Department of Physics and Astronomy, Minnesota State University, Mankato, MN 56001, USA. [3]School of Physics and Astronomy, University of Minnesota, Minneapolis, MN 55455, USA. [4]Space Sciences Laboratory, University of California, Berkeley, CA 94720, USA. [5]Institute of Geophysics and Planetary Physics, Lawrence Livermore National Laboratory, Livermore, CA 94550, USA.

*To whom correspondence should be addressed. E-mail: pepin001@umn.edu